Accepted by IEEE Transactions on Smart Grid (DOI: 10.1109/TSG.2020.2992802)

Optimized Autonomous Operation Control to Maintain the Frequency, Voltage and Accurate Power Sharing for DGs in Islanded Systems

Li Sun, *Student Member, IEEE,* Kai Sun, *Senior Member, IEEE,*
Yunhe Hou, *Senior Member, IEEE,* and Jiabing Hu, *Senior Member, IEEE*

***Abstract*—Most of the launched power electronics-enabled distributed generators (DGs) adopt phase-locked-loop (PLL) synchronization control. In this paper, we delve into two different autonomous operation control (AOC) strategies to ensure the frequency/voltage profile and accurate power sharing for such DGs in islanded systems. The commonly used AOC is based on the concept of active power-frequency ($P-f$) and reactive power-voltage magnitude ($Q-V$) droop and deployed in a decentralized way. It is frequently criticized for inaccurate reactive power sharing between DGs, subject to the mismatch in their output impedances. To cope with this issue, we first design a local AOC using the $P-f$ and $Q-\dot{V}$ (i.e., the time derivate of V) droop concept, where the desired reactive power sharing can be achieved at the expense of a marginal and allowable V excursion. Then, we develop an optimization-based AOC that is implemented through a continuous-time alternating direction method of multipliers (ADMM) algorithm and neighborhood communication. Equilibrium analysis and local asymptotic stability of the proposed AOC strategies are both established using a Lyapunov method. Finally, simulations are carried out in two islanded systems to validate the improvement in power sharing under a wide range of possible system conditions.**

***Index Terms*—ADMM, autonomous operation control (AOC), distributed generators (DGs), droop control, islanded systems.**

NOMENCLATURE

$P,\ Q$	Active and reactive power leaving the bus
$P_L,\ Q_L$	Active and reactive load power
$\omega/f,\ \theta$	Real output frequency and phase angle
$V,\ \omega_0$	Voltage magnitude and normal output frequency
$J,\ D_p,\ D_q$	Virtual inertia and Droop control parameters
$D_{Lp},\ D_{Lq}$	Droop coefficients of loads
$k_p,\ k_q$	f and $\dot{V}$ restoration control parameters
$\boldsymbol{P},\ \boldsymbol{Q},\ \boldsymbol{P_L},\ \boldsymbol{Q_L}$	Vector with entries $P_i,\ Q_i,\ P_{Li},\ Q_{Li}$
$\boldsymbol{V},\ \boldsymbol{\omega},\ \boldsymbol{\theta}$	Vector with entries $V_i,\ \omega_i,\ \theta_i$
$[\boldsymbol{J}],\ [\boldsymbol{D_p}],\ [\boldsymbol{D_q}]$	Diagonal matrix with entries $J_i,\ D_{pi},\ D_{qi}$
$[\boldsymbol{D_{Lp}}],\ [\boldsymbol{D_{Lq}}]$	Diagonal matrix with entries $D_{Lpi},\ D_{Lqi}$
$[\boldsymbol{k_p}],\ [\boldsymbol{k_q}]$	Diagonal matrix with entries $k_{pi},\ k_{qi}$
$m,\ n-m$	The number of DGs and loads
Superscripts and subscripts:	
r	Reference value of variables
$*$	Variables at the system equilibrium point
$i,\ j,\ k$	Serial number
$g,\ d$	Variables for DGs and loads
$p,\ q$	Active and reactive components of variables

Acronyms:

ADMM	Alternating direction method of multipliers
AOC	Autonomous operation control
CAOC	Conventional autonomous operation control
DG	Distributed generator
NAOC	Novel autonomous operation control
OAOC	Optimization-based autonomous operation control
PLL	Phase-locked-loop

This work was supported National Natural Science Foundation of China under Grant 51677160, the Research Grants Council of Hong Kong under Grant GRF17207818, and the Research Grants Council of Hong Kong through the Theme-based Research Scheme under Project No. T23-701/14-N.

L. Sun and Y. Hou are with the Department of Electrical and Electronic Engineering, HKU, Hong Kong (e-mail: sunli@eee.hku.hk; yhhou@eee.hku.hk)

K. Sun is with the Department of EECS, the University of Tennessee, Knoxville, TN 37996, USA (email: kaisun@utk.edu)

J. Hu is with State Key laboratory of Electrical and Electronic Engineering, HUST, Wuhan 430074, China (e-mail: j.hu@mail.hust.edu.cn).

I. INTRODUCTION

With the booming of renewables, distributed generators (DGs) that are responsible for performing the power uptake from renewables and the power delivery to loads have been increasingly integrated in power grids [1], [2]. A common characteristic of DGs is that they are interfaced to the power grid through power electronic converters. The high flexibility and controllability of converters enable DGs to encompass a wide range of operation patterns, from grid connection to small-scale system clustering, and further on islanded operation.

For grid-connected operation, a DG is presently configured with minimum functionalities and without any advanced capability. It commonly adopts the synthesis of the decoupled dq-vector control and phase locked loop (PLL) synchronization control [3]. The output frequency is generated with two portions of the internal feedback loop: (i) the decoupled power control in converters (Path 1), and (ii) the PLL (Path 2) [4]. A negative feedback for the output frequency is formed by Path 1 together with the connected grid; Path 2 creates a positive frequency feedback that drives the output frequency continuously accelerating or decelerating [5]. Once the DG operates in the islanded mode, the positive frequency feedback would incur a monotonous increase/decrease in the output frequency, or even frequency collapses. Beyond this, the power sharing issue is also crucial since DGs are often geographically dispersed and have limited capabilities in providing active/reactive power (and hence frequency/voltage) support.

To resolve the issues associated with DGs in islanded operation, a strict adherence to autonomous frequency/voltage regulation and accurate power sharing (according to their ratings) is required and enforcement is needed. Thus, the autonomous operation control (AOC) has become an indispensable part of DGs in islanded operation. AOC is conventionally built on active power-frequency ($P-f$) and reactive power-voltage magnitude ($Q-V$) droop concept [6], [7], and implemented in a decentralized way [2]. $P-f$ droop control provides a negative frequency feedback to counteract side effects of the positive frequency feedback (caused by Path 2). Since the

frequency features a grid-wide behavior, an even active power sharing between DGs is concomitantly guaranteed. In contrast, $Q-V$ droop control is capable of restoring the voltage level of DGs, but it is impossible to maintain an accurate reactive power sharing in most cases. This is because that the voltage varies with the shared power grid impedance (seen from the connecting DGs). And, such shared impedance is subject to (i) the out-side LCL-filter impedance that is reference to network conditions and performance specifications in the design [8], [9] and (ii) and the line impedance that features mismatch between parallel-connected DGs [10].

Some effort has been made in addressing the inaccurate power sharing issue for grid-forming DGs in islanded systems [11]. The energy source of DGs are modeled by a stiff dc voltage source and the grid-forming capability is performed through virtual synchronization control (with PLL cast off) [12]. In the case where communication is lost, AOC is generally combined with some compensation strategies to preserve the power sharing accuracy [13], [14]. In [13], a compensation loop estimating the online impedance voltage drop effect is established to offset the mismatches among the shared power system impedances by DGs. [14] develops a virtual framework structure-based method to ensure the $P-f/Q-V$ regulation and accurate power sharing. Notably, a virtual inductor is configured at the interfacing inverter output for active and reactive power decoupling and output-voltage regulation [13], [14], and meanwhile the knowledge of grid-connected operation or loads is required. A variation that is $P-f$ and $Q-\dot{V}$ (i.e., the time derivative of V) droop concept is proposed by [15], [16]. The $Q-\dot{V}$ loop makes the reactive power sharing less dependent on the voltage drop associated with the line impedance.

On the other hand, AOC can be implemented in co-ordination with local communication networks to optimize the control performance. Distributed control methods have received most attention due to high reliability, scalability and low cost. In [17], the $Q-V$ droop is complemented with a voltage correction that is generated by a distributed-averaging PI control. The complemented term can be designed to achieve either voltage regulation, reactive power sharing, or a compromise between the two.

However, the power sharing issue associated to PLL-synchronization control-based DGs that inherently have no grid-forming capability is still but should not be underestimated. Inspired by the pioneer work regarding AOC, this paper proposes two different AOC strategies to empower the grid-forming capability and maintain an accurate power sharing for such DGs in islanded systems. The proposed AOCs are built on the $P-f$ and $Q-\dot{V}$ (i.e., the time derivate of V) droop concept, since it could make the power sharing independent of anything but local information, and mitigate the threat of voltage distortion [15]. We then summarize the main features of the proposed controls as follows:

- To the best of the authors' knowledge, this paper is the first to propose the control methods for both frequency, voltage restoration, and accurate power sharing of PLL synchronization control-based DGs in islanded systems, taking into consideration an inability of such DGs to provide grid-forming support and an advantage of $P-f$ and $Q-\dot{V}$ droop concept in improving power sharing accuracy.
- In terms of the proposed novel AOC (NAOC), it has a $P-f$ loop to generate the desired power correction for DGs, which imitates a second-order process using the frequency measurement (from PLL) as the input. The grid-forming capability is built through an inertia and droop control, and additionally an f-restoration supplement that preserves the post-disturbed settling frequency at its nominated value. By contrast, a $Q-\dot{V}$ loop is used to rewrite the reactive power setpoint and has a similar structure to that developed by [15]. The difference is that $\dot{V}$ here is normalized by V to reduce the impact of the voltage magnitude transients on the $Q-\dot{V}$ output.
- In terms of the proposed optimization-based AOC (OAOC), it has advantages in dealing with the issues under conditions of highly loose network and heavily loading conditions. To resolve the consensus averaging OAOC problem (built on the AOC objectives), a continuous-time version of distributed alternating direction method of multipliers (ADMM) algorithm is built to develop the control law of OAOC. OAOC describes the behaviors of continuous dynamic systems. Also, it preserves the superior convergence rate and resilience noises of ADMM algorithms, making it better than the distributed-averaging PI control.

Then, a Lyapunov method is recalled to examine the asymptotic behavior of the close-loop trajectories for an islanded system when NAOC or OAOC engages. Finally, we verify the effectiveness of the proposed strategies in two 6-DG islanded systems, using the MATLAB/SimPowerSystems toolbox.

The remainder of this paper is organized as follows. Section II introduces some technical backgrounds, including network model description, DG control review and AOC objective formulation. A local $P-f$ and $Q-\dot{V}$ droop-based AOC (i.e., NAOC) is developed in Section III. Also, we conduct a stability analysis on the islanded system when NAOC engages. In Section IV, the principle and stability analysis for OAOC embedded in DGs are studied. In Section V, illustrative simulations are conducted on a 7-bus and a 14-bus islanded system to validate the effectiveness of the proposed controls. Section VI draws the conclusions of this paper.

Notations

Let $\mathbf{0}_n$ be the zero vector, $\mathbf{1}_n$ the one vector and $\boldsymbol{I}_n$ the $n\times n$ identity matrix. For a square matrix $[\boldsymbol{A}]$, $[\boldsymbol{A}]<(>)\ 0$ declares that $[\boldsymbol{A}]$ is symmetric negative (positive) definite.

II. Backgrounds

A. Network Model Description

An islanded system consisting of m DGs and $n-m$ loads is considered in this context. We use the set of $\mathcal{N}:=1,\ldots,m$ corresponding to DG agents, whilst $\mathcal{N}_{\mathcal{L}}:=\ m+1,\ldots,n$ representing load agents. In what follows, we leverage the *network-preserving model* [18], [19] to represent all grid components, so that the model identity can be preserved no

matter when DGs (see Section III/IV), loads and transmission lines are involved. This gives a convenient way to seek out the physical insights among different components.

Assumption 1: All the transmission lines are lossless and all involved loads are $f/\dot{V}$ dependent.

1) Power injections at each bus: Consider that two nodes i and j in the islanded system are linked by a nonzero susceptance B_{ij} (> 0). The knowledge of power flow equations [20] admits that the total active (P_i) and reactive power (Q_i) leaving the ith bus through transmission lines are

$$P_i = \sum_{j=1}^{n} V_i V_j B_{ij} \sin\theta_{ij};\ Q_i = -\sum_{j=1}^{n} V_i V_j B_{ij} \cos\theta_{ij} \quad (1)$$

for $\forall i \in \mathcal{N} \cup \mathcal{N}_{\mathcal{L}}$. θ_i and V_i are associated to the phase angle and voltage magnitude of each bus $i \in \mathcal{N} \cup \mathcal{N}_{\mathcal{L}}$; and the common shorthand $\theta_{ij} = \theta_i - \theta_j$ is used.

2) Loads: The field measurement studies in [18], [21] declare that the active (P_{Li}) and reactive (Q_{Li}) components of loads are usually doomed to be with frequency and voltage dependencies, respectively. P_{Li} and Q_{Li} are accordingly restricted to satisfy [22]

$$P_{Li} = -P_i - D_{Lpi}\dot{\theta}_i;\ Q_{Li} = -Q_i - D_{Lqi}\dot{V}_i \quad (2)$$

where D_{Lpi} and D_{Lqi} are dependencies of real power load on the frequency and reactive power load on the time derivative of voltage magnitude; they are positive and small enough [22]. The dynamic loads (like induction machines) are not considered in this context due to their dynamic complexity and difficulty in mathematical and analytical studies. Studies of this are left to future research.

B. Basic Configuration of DGs

Driven by diverse energy paradigms, DGs in islanded systems may represent wind turbines, photovoltaic (PV) arrays or electric vehicles. The dc link bridges the physical and electrical parts of DGs but decouples their dynamics. It promises that a power source (P_{ini}) is able to represent the physical part, as shown in Fig. 1. The electrical part achieves decoupled active and reactive power (PQ)-control through a dual-loop cascaded control (including power control and voltage & current control) [7]. Meanwhile, PLL is used to realize the synchronization of DGs with the external grid. DGs with this typical control configuration are naturally insensible to operating perturbations due to the inability to provide active/reactive power (and hence frequency/voltage) support.

In an islanded system, it is requisite that DGs are capable of performing $P-f$ and $Q-V$ regulation in an autonomous fashion through AOC. At first, DGs should be operating with a predefined power margin in the steady state, which allows DGs to offset their output power for load sharing and frequency/voltage restoration purpose during the post-disturbed state. Then, the output u_{poi} (respectively, u_{qoi}) of AOC is used to rewrite the power setpoint P_{ini} ($P_{ini} = P_i^r - u_{poi}$, respectively, $Q_{ini} = Q_i^r - u_{qoi}$) for the ith DG based on the frequency (respectively, voltage magnitude) information. Notably, the time constant of AOC should be much larger than that of the inner voltage & current control, which is commonly selected in the range of 10 of the time constant of the inner control [23], [24]. Also, the dynamic of dc link is considerably fast. As a result, $P_{ini} = P_i$ (respectively, $V_i^r = V_i$ and $\dot{V}_i^r = \dot{V}_i$) when we focus on the AOC implementation (detailed in Section III and IV).

C. AOC Objectives for DGs

DGs are responsible for maintaining the power balance in the islanded system against disturbances from generation/load patterns. Any power imbalance would cause an excursion in the frequency/voltage magnitude that should be restored until DGs arrive at the desired post-disturbed stable state. Inspired by [15], the $P-f$ and $Q-\dot{V}$ concept is adopted for AOC implementation, which involves the following two issues:

- Guarantee the frequency and voltage magnitude reaching their allowable values in the post-disturbed steady state. In this sense, DGs operate in synchronous mode and have the stable operation point

$$\dot{\theta}_i := \omega_i - \omega_0,\ \text{and}\ \dot{V}_i = 0, \forall i \in \mathcal{N} \cup \mathcal{N}_{\mathcal{L}} \quad (3)$$

  where V_i and θ_i are the bus voltage magnitude and angle, respectively; ω_0 and ω_i are the nominated grid frequency and the output frequency of the ith DG, respectively. Notably, ω_i has the same unit value as f_i, and thereby they are cast as indiscriminate in this context.
- Achieve an accurate active and reactive power sharing between DGs. As such, each DG endeavors to take the power sharing at the same percent of its rated capacity. More particularly, for an islanded system paired with a communication network, the control objective can also be formulated as

$$P_i/P_i^r = P_j/P_j^r,\ \text{and}\ Q_i/Q_i^r = Q_j/Q_j^r, \forall i,j \in \mathcal{N}_i \quad (4)$$

  where $j \in \mathcal{N}_i$ means that the jth DG can communicate with the ith DG.

III. NAOC through Local $P-f$ and $Q-\dot{V}$ Droop

A. Mechanism and Model Description

In this section, we leverage the $P-f$ and $Q-\dot{V}$ droop concept and local f/V measurements to establish a novel AOC

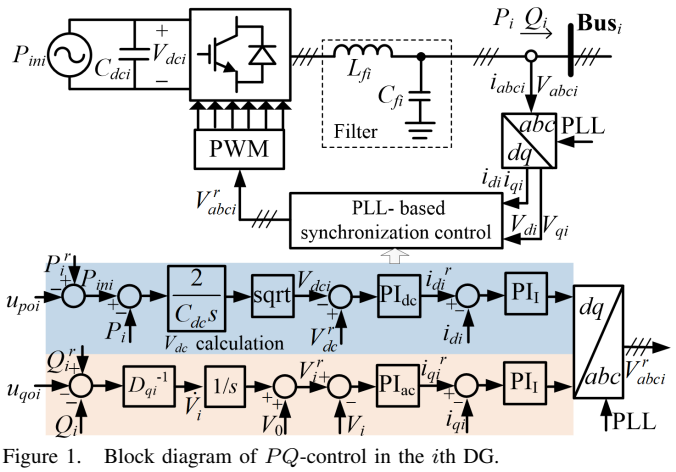

Figure 1. Block diagram of PQ-control in the ith DG.

(namely, NAOC) for DGs. As shown in Fig. 2, its input (f/V) goes through the appended virtual inertia, the $P-f/Q-\dot{V}$ droop and $f/\dot{V}$ restoration block to generate a desired power correction u_{po}/u_{qo}. Therein, virtual inertia block is used to address the stability issues associated with the deteriorating of system inertia and frequency transients in islanded systems. The $P-f$ and $Q-\dot{V}$ droop block is committed to resolving the problem of accurate power sharing [15], [25], with leaving a steady-state error in $f/\dot{V}$. Such an error will be dispelled after it going through the $f/\dot{V}$ restoration block.

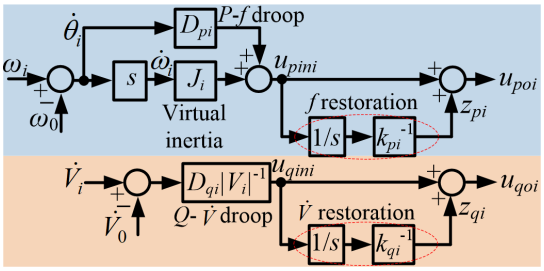

Figure 2. Control block of NAOC for the ith DG.

In what follows, we engage to examine the behavior and stability of DGs applied in islanded systems when NAOC is deployed to fulfill the control objectives (see Section II. C). Before moving on, some mild assumptions are further made:

Assumption 2: All fast dynamics of DGs are discarded hereafter: $P_{ini}=P_i$ and $\dot{V}_i^r=\dot{V}_i$; All DGs operate with a certain power margin in steady state and can offset their power output for all possible load perturbations.

Therefore, for the ith DG, its structure-preserving model is conceived to be

$$\dot{\theta}_i=\omega_i-\omega_0 \tag{5a}$$
$$J_i\dot{\omega}_i+D_{pi}\dot{\theta}_i=P_i^r-P_i-z_{pi} \tag{5b}$$
$$k_{pi}\dot{z}_{pi}=J_i\dot{\omega}_i+D_{pi}\dot{\theta}_i \tag{5c}$$
$$D_{qi}|V_i|^{-1}\dot{V}_i=Q_i^r-Q_i-z_{qi} \tag{5d}$$
$$k_{qi}\dot{z}_{qi}=D_{qi}|V_i|^{-1}\dot{V}_i \tag{5e}$$

where J_i is the virtual inertia constant. D_{pi} and D_{qi} are droop gains for PQ-control. z_{pi} and z_{qi} are auxiliary variables to restore $\dot{\theta}_i$ and $\dot{V}_i$ when regulating the frequency and voltage magnitude. k_{pi} and k_{qi} are parameters associated with the auxiliary variables.

B. Stability Analysis

To facilitate the stability analysis, a compact representation of the closed-loop model for the islanded system is first established in matrix form, see

$$\dot{\boldsymbol{\theta}}_g=\boldsymbol{\omega}_g-\omega_0\mathbf{1}_m \tag{6a}$$
$$[\boldsymbol{J}]\dot{\boldsymbol{\omega}}_g+[\boldsymbol{D}_p]\dot{\boldsymbol{\theta}}_g=\boldsymbol{P}^r-\boldsymbol{P}_g-\boldsymbol{z}_p \tag{6b}$$
$$[\boldsymbol{k}_p]\dot{\boldsymbol{z}}_p=[\boldsymbol{J}]\dot{\boldsymbol{\omega}}_g+[\boldsymbol{D}_p]\dot{\boldsymbol{\theta}}_g \tag{6c}$$
$$[\boldsymbol{D}_q][\boldsymbol{V}_g]^{-1}\dot{\boldsymbol{V}}_g=\boldsymbol{Q}^r-\boldsymbol{Q}-\boldsymbol{z}_q \tag{6d}$$
$$[\boldsymbol{k}_q]\dot{\boldsymbol{z}}_q=[\boldsymbol{D}_q][\boldsymbol{V}_g]^{-1}\dot{\boldsymbol{V}}_g \tag{6e}$$
$$[\boldsymbol{D}_{Lp}]\dot{\boldsymbol{\theta}}_d=-\boldsymbol{P}_L-\boldsymbol{P}_d \tag{6f}$$
$$[\boldsymbol{D}_{Lq}]\dot{\boldsymbol{V}}_d=-\boldsymbol{Q}_L-\boldsymbol{Q}_d \tag{6g}$$

where (6a)-(6e) and (6f)-(6g) are referring to DGs and loads, respectively. The subscripts g and d denote the variables corresponding to $i\in\mathcal{N}$ and $i\in\mathcal{N}_\mathcal{L}$, respectively; $[\boldsymbol{V}_g]^{-1}$ is the inverse of $[\boldsymbol{V}_g]$.

Remark 1: The closed-loop islanded system (6) possesses a unique equilibrium point (EP) $\boldsymbol{s}^*=(\boldsymbol{\omega}^*,\boldsymbol{\theta}^*,\boldsymbol{z}_p^*,\boldsymbol{V}^*,\boldsymbol{z}_q^*)$. It fulfills $(\boldsymbol{\omega}^*)^T=[(\boldsymbol{\omega}_g^*)^T\ (\boldsymbol{\omega}_d^*)^T]=\omega_0\mathbf{1}_n^T$ and

$$\begin{aligned}&\boldsymbol{P}^r-\boldsymbol{P}_g|_{\boldsymbol{s}^*}=\boldsymbol{z}_p^*,\boldsymbol{z}_p^*=\boldsymbol{\sigma}(\mathbf{1}_m^T\boldsymbol{P}^r-\mathbf{1}_{n-m}^T\boldsymbol{P}_L)\\&\boldsymbol{Q}^r-\boldsymbol{Q}_g|_{\boldsymbol{s}^*}=\boldsymbol{z}_q^*,\boldsymbol{z}_q^*=\boldsymbol{\sigma}(\mathbf{1}_m^T\boldsymbol{Q}^r-\mathbf{1}_{n-m}^T\boldsymbol{Q}_L)\\&\boldsymbol{P}_L+\boldsymbol{P}_d|_{\boldsymbol{s}^*}=\mathbf{0}_{n-m},[\boldsymbol{V}_d]^{-1}(\boldsymbol{Q}_L+\boldsymbol{Q}_d|_{\boldsymbol{s}^*})=\mathbf{0}_{n-m}\end{aligned} \tag{7}$$

where $\boldsymbol{\sigma}=[\boldsymbol{D}_p]\mathbf{1}_m/(\mathbf{1}_m^T[\boldsymbol{D}_p]\mathbf{1}_m)$ and $[\boldsymbol{V}_d]^{-1}$ is the inverse of $[\boldsymbol{V}_d]$ pertaining to $i\in\mathcal{N}_\mathcal{L}$.

Proof: From the fact that $\dot{\boldsymbol{\theta}}_g=\boldsymbol{\omega}_g-\omega_0\mathbf{1}_m$ for all $t>0$ and $i\in\mathcal{N}$, and for $\boldsymbol{\omega}_g^*$ together with (6c), we have

$$[\boldsymbol{D}_p](\boldsymbol{\omega}_g^*-\omega_0\mathbf{1}_m)=0$$

which implies that $(\boldsymbol{\omega}_g^*)^T=\omega_0\mathbf{1}_m^T$. In addition, $(\boldsymbol{\omega}_d^*)^T=\omega_0\mathbf{1}_{n-m}^T$ from the steady-state point of (6f). Thus $(\boldsymbol{\omega}^*)^T=\omega_0\mathbf{1}_n^T$. Furthermore, we have from (6b) and (6f) that

$$\mathbf{1}_m^T\boldsymbol{P}^r-\mathbf{1}_m^T\boldsymbol{z}_p^*=\mathbf{1}_m^T\boldsymbol{P}_g=\mathbf{1}_m^T\boldsymbol{P}^r-\mathbf{1}_{n-m}^T\boldsymbol{P}_L$$

which yields $\boldsymbol{z}_p^*=\boldsymbol{\sigma}(\mathbf{1}_m^T\boldsymbol{P}^r-\mathbf{1}_{n-m}^T\boldsymbol{P}_L)$. It follows from [26] that the equation above has at most one solution $\boldsymbol{z}_p^*$. Similarly, we have the most one solution $(\boldsymbol{z}_q^*)$ of the equations regarding the reactive power balance. It is of interest to note that the unique EP in (7) is in correspondence with the operation point denoted by (3). ■

Theorem 1 (Stability of Equilibrium): Under Assumption 2, the EP $\boldsymbol{s}^*=(\boldsymbol{\omega}^*,\boldsymbol{\theta}^*,\boldsymbol{z}_p^*,\boldsymbol{V}^*,\boldsymbol{z}_q^*)$ in the sense of Remark 1 for the system (6) is locally asymptotically stable.

Proof: The stability claim can be established by invoking the Theorem 2.5 in [26]. Inspired by [26], [27], the following incremental Lyapunov function candidate is selected

$$\varepsilon_1(\widetilde{\boldsymbol{s}})=W_1(\widetilde{\boldsymbol{\omega}})+W_2(\widetilde{\boldsymbol{\theta}})+W_3(\widetilde{\boldsymbol{z}}_p)+W_4(\widetilde{\boldsymbol{V}})+W_5(\widetilde{\boldsymbol{z}}_q) \tag{8}$$

$$\begin{aligned}W_1(\widetilde{\boldsymbol{\omega}})&=(1/2)\widetilde{\boldsymbol{\omega}}^T[\boldsymbol{J}]\widetilde{\boldsymbol{\omega}}\\W_2(\widetilde{\boldsymbol{\theta}})&=H(\widetilde{\boldsymbol{\theta}})-H(\widetilde{\boldsymbol{\theta}}^*)-(\nabla H(\widetilde{\boldsymbol{\theta}}^*))^T(\widetilde{\boldsymbol{\theta}}-\widetilde{\boldsymbol{\theta}}^*)\\W_3(\widetilde{\boldsymbol{z}}_p)&=(1/2)\widetilde{\boldsymbol{z}}_p^T[\boldsymbol{D}_p]^{-1}[\boldsymbol{k}_p]\widetilde{\boldsymbol{z}}_p\\W_4(\widetilde{\boldsymbol{V}})&=(\boldsymbol{R}-\boldsymbol{R}^*)^T(\boldsymbol{V}-\boldsymbol{V}^*)\\W_5(\widetilde{\boldsymbol{z}}_q)&=(1/2)\widetilde{\boldsymbol{z}}_q^T[\boldsymbol{D}_q]^{-1}[\boldsymbol{k}_q]\widetilde{\boldsymbol{z}}_q\end{aligned}$$

where $\boldsymbol{R}$ is a vector with entries $R_i:=-\sum V_jB_{ij}\cos\theta_{ij}$; in addition, $\widetilde{\boldsymbol{\omega}}_{\boldsymbol{g}}=\boldsymbol{\omega}_g-\boldsymbol{\omega}_g^*$, $\widetilde{\boldsymbol{\theta}}=\int_0^\tau\widetilde{\boldsymbol{\omega}}d\tau$, $\widetilde{\boldsymbol{z}}_p:=\boldsymbol{z}_p-\boldsymbol{z}_p^*$, $\widetilde{\boldsymbol{z}}_q:=\boldsymbol{z}_q-\boldsymbol{z}_q^*$, and $H(\boldsymbol{\theta})=-(1/2)\sum V_iV_jB_{ij}\cos\theta_{ij}$, for convenience. In (8), W_1 (≥ 0), W_2 (≥ 0) and W_4 (≥ 0) are conveniently recast as the kinetic energy, network potential energy, and load potential energy, respectively (according to [27]), and thus they are positive; in addition, $W_3\geq 0$ and $W_5\geq 0$. We consequently have that ε_1 is positive except for the EP, where $\varepsilon_1=0$.

Differentiating ε_1 subject to the constraint manifold defined by (7) yields

$$\dot{\varepsilon_1}=\dot{W}_1+\dot{W}_2+\dot{W}_3+\dot{W}_4+\dot{W}_5 \tag{9}$$

where

$$\dot{W}_1 = \widetilde{\boldsymbol{\omega}}^T[\boldsymbol{J}]\dot{\widetilde{\boldsymbol{\omega}}}, \quad \dot{W}_2 = (\nabla H(\widetilde{\boldsymbol{\theta}}) - \nabla H(\widetilde{\boldsymbol{\theta}}^*))^T\dot{\widetilde{\boldsymbol{\theta}}}$$
$$\dot{W}_3 = \widetilde{\boldsymbol{z}}_p^T[\boldsymbol{D}_p]^{-1}[\boldsymbol{k}_p]\dot{\widetilde{\boldsymbol{z}}}_p, \quad \dot{W}_4 = (\boldsymbol{R} - \boldsymbol{R}^*)^T\dot{\boldsymbol{V}}$$
$$\dot{W}_5 = \widetilde{\boldsymbol{z}}_q^T[\boldsymbol{D}_q]^{-1}[\boldsymbol{k}_q]\dot{\widetilde{\boldsymbol{z}}}_q$$

Using (6) and assuming that the fast dynamics of $\dot{\boldsymbol{\omega}}_g$ already end in comparison to $\dot{\boldsymbol{z}_p}$ for (6c), we have

$$\dot{\varepsilon_1} = -\widetilde{\boldsymbol{\omega}}^T[\boldsymbol{D}_p]\widetilde{\boldsymbol{\omega}} - \dot{\boldsymbol{V}}^T[\boldsymbol{D}_q][\boldsymbol{V}_g]^{-2}\dot{\boldsymbol{V}} \leq 0 \tag{10}$$

In order to establish asymptotic stability, we observe that the above arguments also have the following implication

$$\dot{\varepsilon_1} \equiv 0 \Longleftrightarrow \widetilde{\boldsymbol{\omega}} \equiv \boldsymbol{0}_m, \ \dot{\boldsymbol{V}} \equiv \boldsymbol{0}_m \tag{11}$$

given that $[\boldsymbol{D}_p]$ and $[\boldsymbol{D}_q]$ are both nonzero (since the pertinent DGs are required to install AOC). Thus, the invariant set $\dot{\varepsilon_1} \equiv 0$ is an equilibrium set. By virtue of the Theorem 2.5 in [26], the unique equilibrium $\boldsymbol{s}^*$ is asymptotically stable. ■

Assumption 3: The uniform droop gain ratio is required to guarantee accurate power sharing [28]. That is, the ratio D_{pi}/P_i^r and D_{qi}/Q_i^r are both constant for all $i \in \mathcal{N}$.

Main result: The remark below establishes a consensus representation of the objectives (3) and (4) and is fundamental for the optimization-based auxiliary power control proposed in the following section.

Remark 2: Consider the system (6) with Assumption 3, the stable EP $(\boldsymbol{\omega}^*, \boldsymbol{\theta}^*, \boldsymbol{z}_p^*, \boldsymbol{V}^*, \boldsymbol{z}_q^*)$ settled by the objectives (3) and (4) must also fulfill

$$D_{xi}^{-1}(X_i^r - X_i^* - z_{xi}^*) = 0 \tag{12a}$$
$$D_{xi}^{-1}z_{xi}^* = D_{xj}^{-1}z_{xj}^* \tag{12b}$$

where $i, \ j \in \mathcal{N}$ and X/x represent either the notions for P/p or Q/q.

Proof: The fast dynamics of $\dot{\boldsymbol{\omega}}_g$ are assumed to already end with respect to the dynamics of $\dot{\boldsymbol{\theta}}_g$ and each element of $\boldsymbol{V}^*$ possesses a unit value. At first, manipulating the steady-state representations of (5b) and (5d) yields (12a). Then, the following equations are derived from (5b) and (5d) by dividing with P_i^r and Q_i^r, respectively,

$$P_i/P_i^r = 1 - (D_{pi}/P_i^r)(z_{pi}^*/D_{pi}) - (D_{pi}/P_i^r)\dot{\theta}_i^* \tag{13a}$$
$$Q_i/Q_i^r = 1 - (D_{qi}/Q_i^r)(z_{qi}^*/D_{qi}) - (D_{qi}/Q_i^r|V_i^*|)\dot{V}_i^* \tag{13b}$$

Consider that $\dot{\theta}_i$ and $\dot{V}_i$ for $i \in \mathcal{N}$ would coincide at a stable EP. From (13), the objective (4) can be accordingly reformulated as (12b) under the Assumption 3. ■

IV. OAOC THROUGH ADMM IMPLEMENTATION

Although the proposed NAOC (built on $P-f$ and $Q-\dot{V}$ droop concept) outperforms the conventional AOC (built on $P-f$ and $Q-V$ droop concept) in accurate power sharing, such control performance may still not be guaranteed under the conditions of (i) highly loose network and (ii) heavily loading conditions. To circumvent this issue, we try to build the control objectives (3) and (4) as an optimization problem and solve it using a continuous-time ADMM algorithm in this section.

A. Communication Network Description

Each DG agent is capable to conduct some local computations and neighboring communication. The communication network is naturally modeled as an undirected and connected graph $\mathcal{G}(\mathcal{N}, \mathcal{E})$, where the edges in $\mathcal{E}$ represent pairs of agents that can communicate. Agent $i \in \mathcal{N}$ communicates with the single-hop agents in its neighborhood $\mathcal{N}_i$. The adjacent matrix $[\boldsymbol{A}]$ with weights $w_{ij} = 1$ if $j \in \mathcal{N}_i$, and $w_{ij} = 0$ otherwise.

B. Mechanism of OAOC

Recalling (12) in Remark 2, the prime variable z_{xi} is the local estimation of $X_i^r - X_i$ under the concept of ADMM algorithm. One possible reformulation of (12) can be written as the following consensus optimization problem:

$$\min \sum_{i=1}^{m} \|D_{xi}^{-1}((X_i^r - X_i) - z_{xi})\| \tag{14a}$$
$$\text{s.t. } D_{xi}^{-1}z_{xi} = D_{xj}^{-1}z_{xj}, \ \forall j \in \mathcal{N}_i \tag{14b}$$

Following the average-consensus theorem given in [29], the optimizers for (14) provide the following result

$$D_{xi}^{-1}z_{xi}^* = (1/m)\sum_{i=1}^{m} D_{xi}^{-1}(X_i^r - X_i) \tag{15}$$

Using (15) to substitute $D_{xi}^{-1}z_{xi}^*$ in (13) yields the power sharing ratios for $\forall i \in \mathcal{N}$ with satisfying

$$X_i/X_i^r = 1 - (D_{xi}/mX_i^r)\sum_{i=1}^{m} D_{xi}^{-1}(X_i^r - X_i) \tag{16}$$

As such, it admits to achieve the objectives of both (3) and (4) through solving the optimization problem presented by (14). In what follows, we propose to solve the problem (14) using the ADMM algorithm, taking into consideration its superior convergence rate and resilience to communication noises [30].

[30] develops a discrete-time version of the ADMM-based consensus algorithm which has two implementations: Method A and Method B. Method A (represented by equations (6)-(7) in [30]) uses two message exchanges, meaning that the communication from a two-hop-neighbors is required. Method B (represented by equations (6)-(10) in [30]) uses a unique (i.e., single-hop) message exchange. On this basis, a continuous-time version of ADMM for solving (14) will be built and integrated into the control law (5). The reader is also referred to [31] for a study on ADMM applied in continuous dynamic systems.

The dynamics of z_{pi} and z_{qi} under two ADMM implementations can be estimated using

$$k_{xi}\dot{z_{xi}} = (1-d_i)(X_i^r - X_i - z_{xi}) + D_{xi}y_{xi} + 2D_{xi}u_{xi} \tag{17}$$

associated with the notation $a_{ij} = w_{ij}/(\sum_{k\in\mathcal{N}_j} w_{kj})$, $b_{ij} = w_{ij}/(1+\sum_{k\in\mathcal{N}_i} w_{ik})$, and $d_i = \sum_{j\in\mathcal{N}_i} b_{ij}$. w_{ij} is the weight for information exchange between the ith and the jth DG. Then, one can implement the OAOC law according to the presented in Fig. 3.

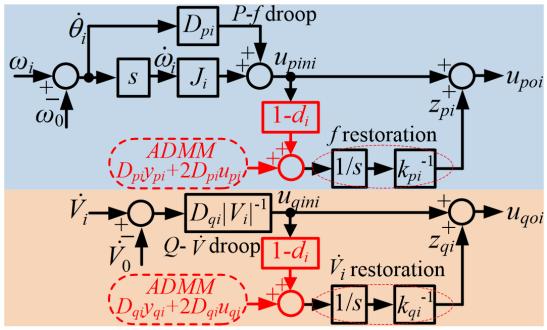

Figure 3. Control block of OAOC for the ith DG.

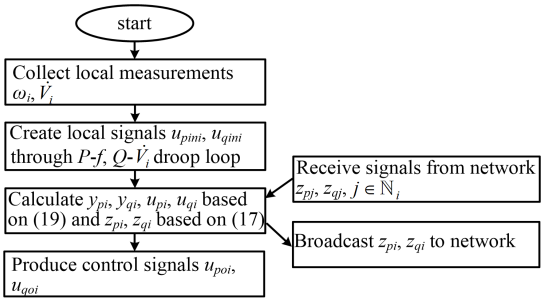

Figure 4. The flowchart of OAOC through ADMM implementation.

In addition, the involved y_{xi} and u_{xi} possess the following dynamics

Method A:

$$\dot{y_{xi}} = u_{xi} = \sum_{j\in\mathcal{N}_i} b_{ij}\Big(\sum_{k\in\mathcal{N}_j} a_{kj}z_{xk}/D_{xk}\Big) - d_i z_{xi}/D_{xi} \quad (18)$$

Method B:

$$\dot{y_{xi}} = u_{xi} = \sum_{j\in\mathcal{N}_i} e_{ij}z_{xj}/D_{xj} - \Big(\sum_{j\in\mathcal{N}_i} e_{ij}\Big)z_{xi}/D_{xi} \quad (19)$$

where $e_{ij} = (1-d_i)(w_{ij}w_{ji})/(w_{ij}+w_{ji})$.

Equations (17) and (18) (or (19)) use differential equations to model the behavior of OAOC in the continuous-time limit, differing from their discrete counterparts (see [30]) that use difference equations to model the behavior of a specific control. However, the convergence of the resulting dynamic system with OAOC matches the known convergence of discrete counterpart, as declared in Remark 3.

Remark 3: (**Convergence**) Provided that (i) the discrete-time version of ADMM algorithm in [30] uses the proper step-size settings and (ii) instead of (5c) and (5e), the control law (17) together with (18) or (19) is integrated into the system (6). The proposed OAOC solves the problem (14).

Proof: It suffices to notice that (i) the consensus averaging optimization problem (14) is a linear quadratic one with a strongly convex objective function; (ii) the existence and feasibility of the desired stable EP pertaining to the system (6) can always be maintained under Assumption 2 [19]. Thus, the stable EP satisfies the optimality criteria of (14). In addition, the embedded ADMM algorithm in OAOC comes from its discrete counterpart. The Theorem 3 in [30] has declared that the convergence of the discrete-time ADMM to its limit value is regulated by a norm-2 bound (see Equation (33) in [30]). Following a theoretical proof (in analogous to Appendix C in [30]), we have that the optimum of (14) can indeed be reached by the proposed control law. ■

Since Method A and Method B perform a similar convergence rate [30], it is advantageous to adopt Method B for the OAOC implementation due to less information exchange and better noise resilience in comparison to Method A. To limit the space, Method B is accordingly used to implement the OAOC law (consisting of (17) and (19)) with the control flow shown in Fig. 4.

C. Stability Analysis

The proposed OAOC requires communication interfaces, where neighboring communication can be realized through low-bandwidth cyber technologies like [32]. It is of interest to point out that if the ADMM-based control law is inactivated (by setting $w_{ij} = 0$, for all i, j), OAOC reduces to NAOC ((5c) and (5e)). In this sense, all trajectories of the system (6) with the OAOC deployed would still converge to one of EPs in sense of Theorem 1. Consequently, the OAOC can be cast as a supplement control action from neighboring DGs.

Remark 4: When OAOC is deployed, the frequency/voltage regulation actions of DGs consists of two phases: the local $P-f$ and $Q-\dot{V}$ control (5) and the distributed ADMM-based control (17) together with (19). It follows that (i) in the early stage, the local $P-f$ and $Q-\dot{V}$ control governs the process of the frequency/voltage restoration and synchronization, fast reaching the first-phase steady-state of the islanded system; and (ii) the ADMM-based control then drives the system into the second-phase with achieving the final desired steady-state.

Theorem 2 (Stability of Equilibrium): Under Assumptions 2 and 3, the EP $\widehat{\boldsymbol{s}}^* = (\boldsymbol{\omega}^*, \boldsymbol{\theta}^*, \boldsymbol{z}_p^*, \boldsymbol{y}_p^*, \boldsymbol{V}^*, \boldsymbol{z}_q^*, \boldsymbol{y}_q^*)$ of the system (6) with OAOC deployed is locally asymptotically stable.

Proof: Based on the conditions described by Remark 4, we choose a new incremental Lyapunov function candidate described as

$$\begin{aligned} \varepsilon &= \varepsilon_1 + \varepsilon_2 + \varepsilon_3 \\ \varepsilon_2 &= (1/2)(\boldsymbol{y}_p^T[\boldsymbol{D}_p]\boldsymbol{y}_p + \boldsymbol{y}_q^T[\boldsymbol{D}_q]\boldsymbol{y}_q) \\ \varepsilon_3 &= (1/2)(-\boldsymbol{z}_p^T[\boldsymbol{k}_p][\boldsymbol{U}]^{-1}\boldsymbol{z}_p - \boldsymbol{z}_q^T[\boldsymbol{k}_q][\boldsymbol{U}]^{-1}\boldsymbol{z}_q) \end{aligned} \quad (20)$$

where ε_1 comes from Section III. B. Apparently, ε_1 and ε_2 are both positive. $\boldsymbol{U}$ is the communication protocol of ADMM-based control in (19). From the Theorem 1 in [30], all the eigenvalues of $\boldsymbol{U}$ are negative but the maximum one is zero. Thus, ε_3 keeps non-negative, so does ε. By taking the total time derivative of ε yields

$$\dot{\varepsilon} = \dot{\varepsilon}_1 - 2(\boldsymbol{z}_p^T[\boldsymbol{D}_p]\boldsymbol{z}_p + \boldsymbol{z}_q^T[\boldsymbol{D}_q]\boldsymbol{z}_q) \quad (21)$$

Combining the proof of Theorem 1 and (21), a negative $\dot{\varepsilon}_1$ hence creates a negative $\dot{\varepsilon}$, so that the EP $\widehat{\boldsymbol{s}}^*$ is locally asymptotically stable. ■

V. Simulation Tests

In order to demonstrate the performance of the proposed controls, two 6-DG islanded systems are adopted to conduct

Table I
PARAMETER SETTINGS FOR DGS' DROOP CONTROL

-	$P-f$			$Q-V$	$Q-\dot{V}$	
-	J	D_p	k_p	D_q	D_q	k_q
CAOC	10	20	-	15	-	-
NAOC	10	20	5	-	10	5
OAOC	10	20	5	-	10	5

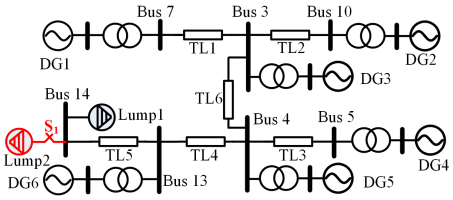

Figure 5. 7-bus 6-DG islanded system.

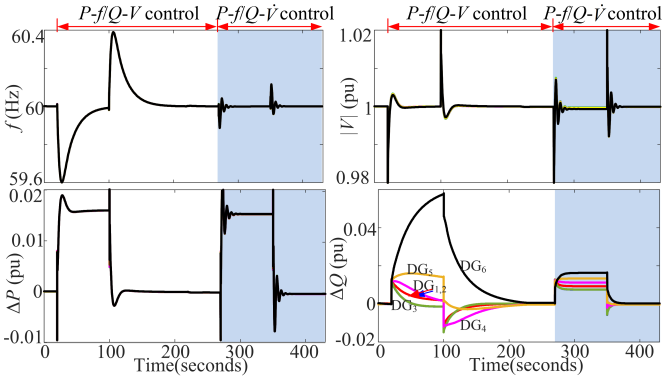

Figure 6. Responses of DGs in tight network, lightly loading conditions.

the simulation tests, as shown in Fig. 5 and Fig. 9. The topologies of them (i.e., 7-bus and IEEE 14-bus modified test systems) respectively refer to [15] and [33] are constructed in MATLAB/Simulink. Each DG is represented by an aggregated 2-MW full-converter wind turbine (refer to [33]), with a rated capacity of 300 MW (150×2 MW). The mechanical system is treated as a power source, while the dynamics of power control, voltage & current control, PLL control and dc link are all simulated. The line parameters are listed as follows: (i) a uniform ratio of R/X settles at $1/10$; (ii) in the 7-bus test system, the impedance is doomed to be tight for 10-km transmission lines or lossy for 100-km transmission lines; (iii) in the 14-Bus test system, the buses are interconnected through 100-km transmission lines.

In our simulations the parameter settings corresponding to $P-f$ and $Q-V$ or $P-f$ and $Q-\dot{V}$ droop are tabulated in Table I. Therein, CAOC is a shorthand for conventional AOC. The adjacent matrix of the communication network for DG1-DG6 is set as

$$[\boldsymbol{A}] = (w_{ij})_{6\times 6} = \rho[\boldsymbol{T}]$$

$$[\boldsymbol{T}] = \begin{bmatrix} 0 & 1/2 & 0 & 0 & 0 & 1/2 \\ 1/2 & 0 & 1/2 & 0 & 0 & 0 \\ 0 & 1/2 & 0 & 1/2 & 0 & 0 \\ 0 & 0 & 1/2 & 0 & 1/2 & 0 \\ 0 & 0 & 0 & 1/2 & 0 & 1/2 \\ 1/2 & 0 & 0 & 0 & 1/2 & 0 \end{bmatrix}$$

where ρ is selected to obtain a minimized convergence speed (refer to, Section V in [30]). Please refer to Appendix for other control parameters regarding DGs.

A. 7-Bus System with A Single Load

In the 7-bus test system, only a single load bus is included. Under lightly loading conditions, each WT has a power output level of 0.479 pu (with a 15% power margin preserved), Lump 1 is 845 MW-j65.6 Mvar and Lump 2 is 30 MW+j20 Mvar (initially disconnected); under heavily loading conditions, each WT has a power output level of 0.840 pu (with a 15% power margin preserved), Lump 1 is 1495 MW-j75.6 Mvar and Lump 2 is 90 MW+j60 Mvar (initially disconnected). Load perturbations are set by closing the switch S_1 at $t = 20$ s (respectively, $t = 270$ s) and reopening S_1 at $t = 100$ s (respectively, $t = 350$ s).

In what follows, there are three major simulations performed: (i) demonstrating the performance of NAOC when the 7-bus system operate with a tight network and light loads; (ii) demonstrating the performance of NAOC when the 7-bus system operate with a loose network and light loads; and (iii) demonstrating the robustness of the proposed AOC strategies to loading conditions.

The simulation results are displayed in Fig. 6 to Fig. 8. Some important findings can be concluded:

- Irrespective of the network structure and loading condition, the frequency and voltage magnitude for all DGs can be preserved at their nominal levels through CAOC or the proposed NAOC/OAOC.
- CAOC has inability to ensure accurate power sharing for DGs. Conversely, NAOC is capable of preserving accurate power sharing between DGs when the test system operates with a tight network and light loads.
- When the test system has a loose network or heavy loads, it is hard to achieve accurate power sharing for DGs through NAOC. This is mainly because that (i) the line impedance itself would play a significant role in the reactive power consumption; (ii) the non-linear behaviors of the test system become considerable under heavily loading conditions.
- The OAOC control is always effective in performing the frequency/voltage restoration and accurate power sharing, subject to a tight/loose network structure and lightly/heavily loading condition. This highly promotes the robustness of DGs' autonomous operation to varying system conditions.

B. 14-Bus System with Multiple Loads

The application of the proposed control in multiple load-bus systems is examined using an IEEE modified 14-bus test system. Three scenarios are set to evaluate the performance of NAOC and OAOC under different network structures or loading conditions. (i) The test system is configured with a topology as shown in Fig. 9; (ii) the test system has a modified topology with the removal of six transmission lines (that link Bus 1-2, Bus 2-4, Bus 2-3, Bus 7-9, Bus 9-14,

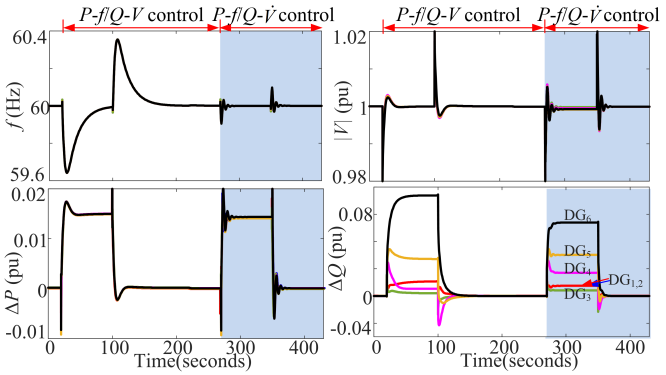

Figure 7. Responses of DGs in loose network, lightly loading conditions.

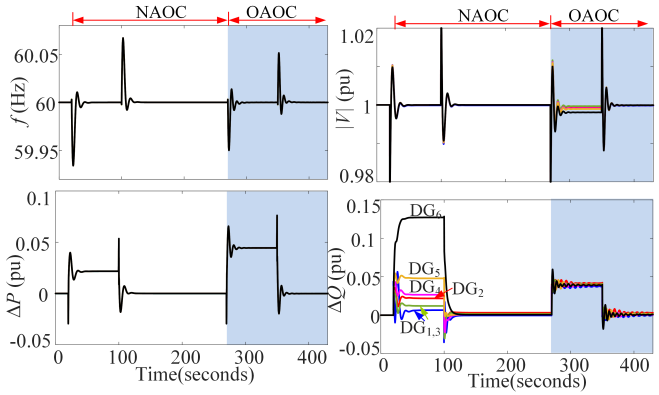

Figure 8. Response of DGs in tight network, heavily loading conditions.

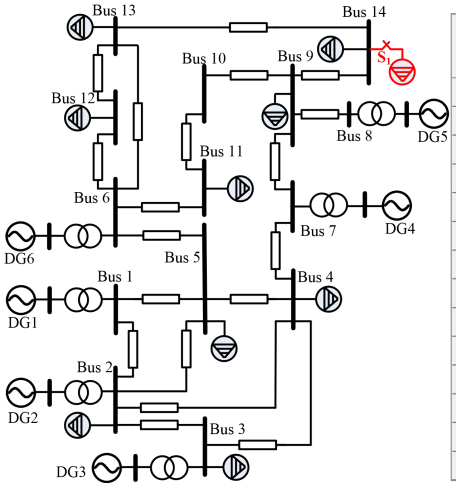

Bus No.	Load Power	
	P (MW)	Q (MVar)
1	–	–
2	53.5	11.4
3	69.5	15
4	46.3	–
5	16.2	–
6	–	–
7	–	–
8	–	–
9	100.3	12.4
10	–	–
11	57.7	1.3
12	133.5	10.8
13	190	-17.6
14	173	-10.5

Figure 9. 14-bus 6-DG islanded system (with the tabulated load power at each bus).

Bus 12-13); (iii) the test system operate in heavily loading conditions (with each load at Bus 9-14 having an increase of 100 MW-j10 Mvar). A load of 30 MW+j20 Mvar under lightly loading conditions (or 90 MW+j60 Mvar under heavily loading conditions) is connected (by closing S_1) to Bus 14 at $t = 20$ s (respectively, $t = 180$ s) and disconnected (by reopening S_1) at $t = 100$ s (respectively, $t = 260$ s). The results are displayed in Fig. 10 to Fig. 12.

Observations from Fig. 10 to Fig. 12 prove that OAOC has advantages over NAOC in control performance, since it

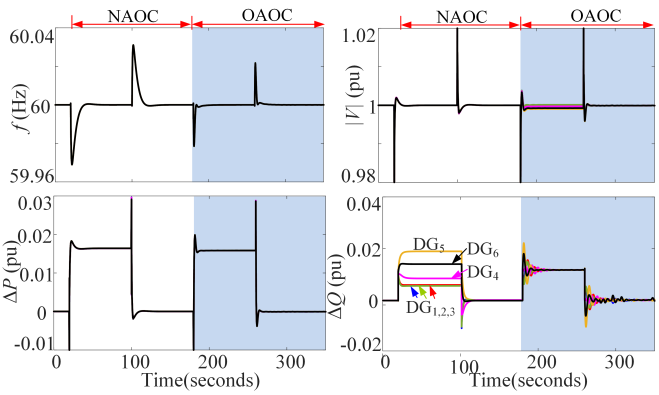

Figure 10. Responses of DGs in 14-bus system with the original topology.

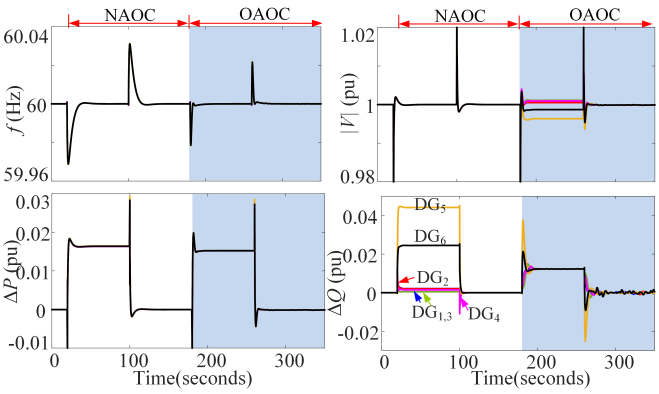

Figure 11. Responses of DGs in 14-bus system with a modified topology.

empowers DGs to ensure the frequency/voltage restoration and accurate load sharing in a wider range of system conditions. Besides, we consider a load perturbation that is created by adding five loads with each being 10 MW+j5 Mvar under lightly loading conditions (or 20 MW+j10 Mvar under heavily loading conditions) to Bus 10-14. The results are similar to Fig. 10 to Fig. 12, and confirm the improvement of power sharing accuracy by OAOC. In addition, Fig. 13 and Fig. 14 further demonstrate the performance of OAOC by considering various DG sizes (where the parameters in Table I are used, but $D_q = 5$ to improve the transients of the reactive power) and control parameters (where DGs have the same size), respectively.

The simulations for DGs with deployment of CAOC are also conducted and plotted. In addition, the simulation scenarios in terms of more diverse network topologies and loading conditions are involved. To save the space, the results are not presented. They still promise that (i) NAOC outperforms the CAOC in terms of maintaining an even power sharing, but possibly fails against some non-ideal system conditions; (ii) however, this issue can be well resolved by the use of OAOC, with the guarantee of a better robustness and resilience to variations in the system condition.

C. Comparative Simulations to Other AOC Strategies

1) Consensus-droop AOC without ADMM implementation: We consider the optimization-based AOC of each DG is

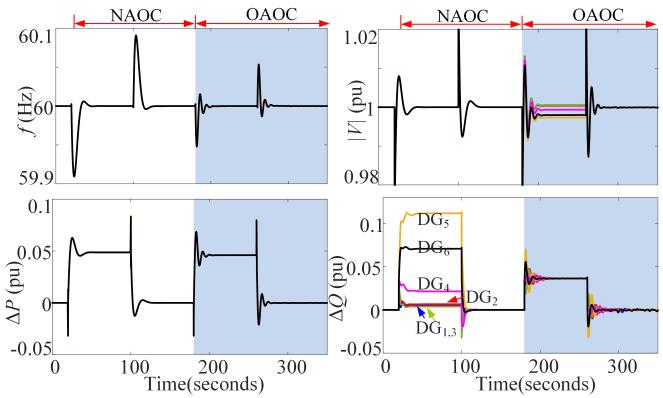

Figure 12. Responses of DGs in 14-bus system with heavy loads.

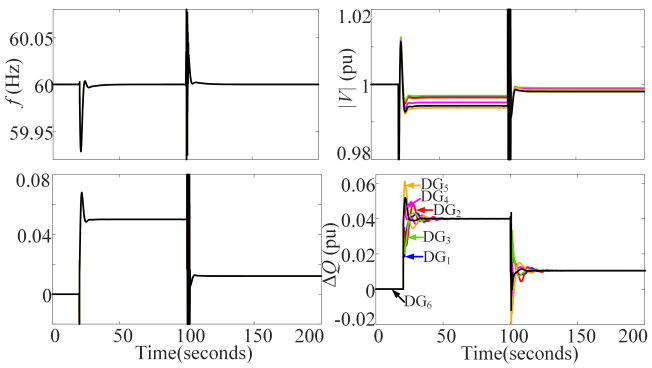

Figure 13. Responses of DGs that have the same OAOC setting but different sizes (DG1-DG6 are rated at 300MW, 200MW, 400MW, 100MW, 500MW and 600MW, respectively).

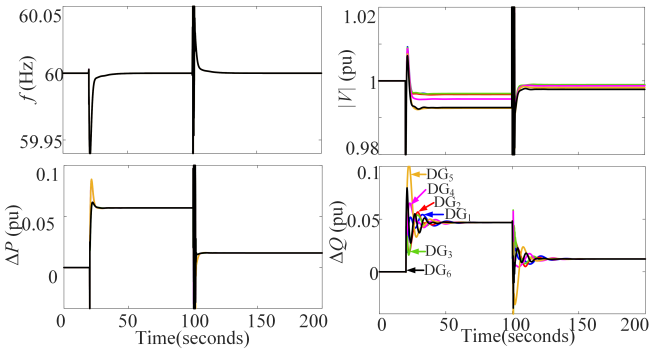

Figure 14. Responses of DGs that have the same size but different OAOC settings (J, D_p/D_q and k_p/k_q for DG1, DG4 and DG5 are changed to be 20, 40/20 and 10/10).

studied by consensus-droop control without ADMM implementation. In this case, the control law is hence written as

$$k_{xi}\dot{z_{xi}} = \sum_{j\in\mathcal{N}_i} w_{ij}(z_{xj}/D_{xj} - z_{xi}/D_{xi}) \tag{22}$$

The values of k_{pi} and k_{qi} are referred to Table I. Unlike (17) and (19), (22) resolves the problem (14) in a simple consensus-averaging way.

Similar to Subsection. B, two scenarios are considered, where the modified IEEE 14-bus test system start from identical initial condition with a tight network then switched to a loose network. A load step of 90 MW+j60 Mvar is created

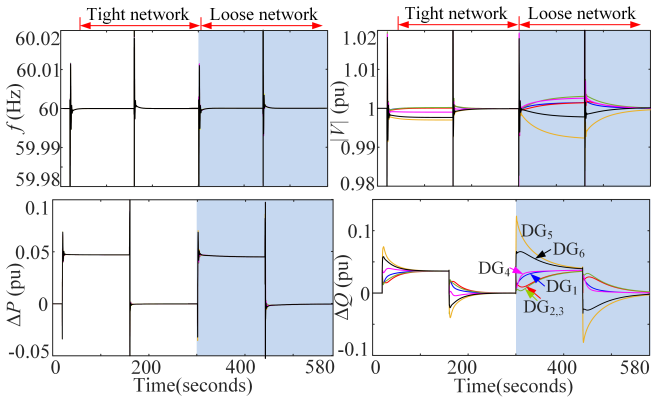

Figure 15. Responses of DGs when consensus-based droop control engages.

by closing S_1 at $t = 20$ s (respectively, $t = 300$ s) and reopening S_1 at $t = 160$ s (respectively, $t = 440$ s). The simulation results are plotted in Fig. 15. Compared to the results in Section V. B, the following important findings can be obtained. Such findings are also applicable when the test system operates under heavily loading conditions, while the simulation results are not displayed here to save space.

- Whether in a tightly or loosely interconnected (lightly or heavily loaded) system, both the proposed OAOC (with ADMM implementation) and the consensus-droop based control empower DGs with the capability of maintaining the operation stability and accurate power sharing.
- The proposed OAOC through ADMM implementation is able to reach accurate power sharing after few seconds, which far faster than the consensus-droop based control. Thus, the islanded system would achieve an enhanced autonomous operation stability through the proposed OAOC.

2) A variant of $P-f$ and $Q-V$ droop control through distributed averaging: In this segment, we try to compare the control performance of the proposed AOC strategies (based on $P-f$ and $Q-\dot{V}$ droop control) and the variants of $P-f$ and $Q-V$ droop control. For instance, the DAPI control in [17] is selected, where the $P-f$ and $Q-V$ loop are both implemented through a distributed averaging algorithm. In the following simulations, the DAPI parameters (with the notations reference to [17])) are set as $k = 0.5, \kappa = 2, m = 0.05, n = 0.1, b = 0.5, \beta = 0.2$.

The simulations are conducted in the modified IEEE 14-Bus system. The perturbed load with 30 MW+j20 Mvar is connected to Bus 14 at $t = 20$ s (respectively, $t = 420$ s) and disconnected at $t = 220$ s (respectively, $t = 620$ s). The simulation results are collected in Fig. 16 (where the simulation results under heavily loading conditions are not displayed). When compared to Fig. 10 to Fig. 12, it promises that (i) OAOC outperforms DAPI in the control efficacy and the convergence rate; and (ii) OAOC has a higher robustness than DAPI to varying system conditions. In addition, it is challenging for parameter settings of DAPI since the distributed voltage control would potentially destabilize the $Q-V$ droop control [17].

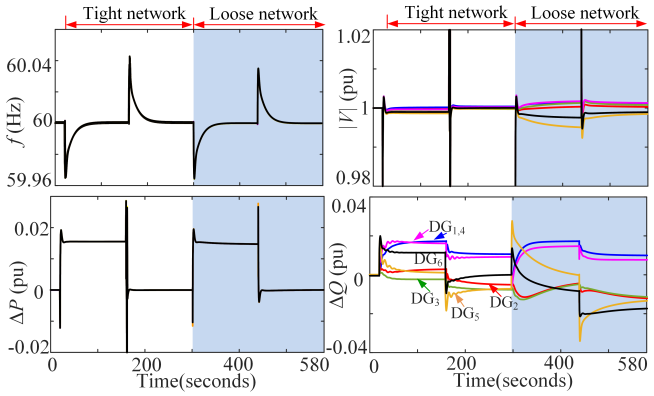

Figure 16. Responses of DGs when DAPI (refer to [17]) engages.

VI. Conclusion

This paper leverages the $P-f$ and $Q-\dot{V}$ droop concept to resolve issues encountered in autonomous frequency/voltage regulation and accurate load sharing for multiple (PLL synchronization controlled) DGs in islanded systems. The outcomes of the study are given as follows. (i) Aside from regulating the frequency/voltage in an autonomous fashion, NAOC using the $P-f$ and $Q-\dot{V}$ droop makes the reactive power of DGs less sensitive to the system impedance mismatch. This enables DGs to perform load sharing accurately in a tightly interconnected and lightly-loading islanded system. (ii) The OAOC built on consensus optimization and ADMM implementation is proposed to circumvent the AOC issues during varying system conditions. In this case, the accurate power sharing between DGs is robust to loose networks and heavily loading conditions. (iii) The asymptotic stability of the islanded system is proved through a Lyapunov method, when NAOC or OAOC is deployed. Simulations conducted on a single load 7-bus and a multiple load 14-bus system demonstrate that OAOC is preferable for preserving autonomous frequency, voltage regulation and accurate power sharing for DGs in a wide range of possible system conditions.

VII. Appendix

DG parameters (on Base of Machine Rating) [33]

$P_n = 2MW, V_n = 575V, \omega_0 = 120\pi$, filter resistance: $R_f = 0.003$, $L_f = 0.15$, dc capacitor: $C = 90000\mu F$, dc voltage: $U_{dc} = 1100V$, terminal-voltage control: $k_{pv} = 1, k_{iv} = 20$, dc voltage control: $k_{pdc} = 1.1, k_{idc} = 27.5$, current control: $k_{pi} = 1, k_{ii} = 50$, PLL control: $k_{pp} = 60, k_{ip} = 1400$.

References

[1] B. Kroposki, B. Johnson, Y. Zhang, V. Gevorgian, P. Denholm, B. M. Hodge, and B. Hannegan, "Achieving a 100% systems with extremely high levels of variable renewable energy," *IEEE Power Energy Mag.*, vol. 15, no. 2, pp. 61-73, Mar. 2017.

[2] D. G. Photovoltaics, and E. Storage, "IEEE standard for interconnection and interoperability of distributed energy resources with associated electric power systems interfaces," *IEEE Std*, pp. 1547-2018, Apr. 2018.

[3] A. Yazdani, and R. Iravani, *Voltage-sourced converter in power systems: Modelling control and application*, New York, NY, USA:Wiley, 2010.

[4] L. Sun, C. Peng, J. Hu, and Y. Hou, "Application of Type 3 wind turbines for system restoration," *IEEE Trans. Power Syst.*, vol. 33, no. 3, pp. 3040-3051, May 2018.

[5] D. Dong, J. Li, D. Boroyevich, P. Mattavelli, I. Cvetkovic, and Y. Xue, "Frequency behavior and its stability of grid-interface converter in distributed generation systems," in *Proc. 2012 IEEE Applied Power Electronics Conf. Expo., IEEE*, pp. 1887-1893, 2012.

[6] A. D. Paquette, M. J. Reno, R. G. Harley, and D.M. Divan, "Sharing transient loads: Causes of unequal transient load sharing in islanded microgrid operation," *IEEE Industry Applications Magazine*, vol. 20, no. 2, pp. 23-34, Mar. 2014.

[7] Y. Zhang and B. T. Ooi, "Stand-alone doubly-fed induction generators (DFIGs) with autonomous frequency control," *IEEE Trans. Power Delivery*, vol. 28, no. 2, pp. 752-760, Apr. 2013.

[8] M. Liserre, F. Blaabjerg, and S. Hansen,"Design and control of an LCL-filter-based three-phase active rectifier," *IEEE Trans. Ind. Appl.*,vol. 41, no. 5, pp. 1281-1291, Oct. 2005.

[9] D. Yang, X. Ruan, and H. Wu, "Impedance shaping of the grid-connected inverter with LCL filter to improve its adaptability to the weak grid condition," *IEEE Trans. Power Electron.*, vol. 29, no. 11, pp. 5795-5805, Nov. 2014.

[10] Sina Parhizi, Hossein Lotfi, Amin Khodaei, Shay Bahramirad, "State of the art in research on microgrids: A review," *Access IEEE*, vol. 3, pp. 890-925, 2015.

[11] H. Han, X. Hou, J. Yang, J. Wu, M. Su, and J. M. Guerrero, "Review of power sharing control strategies for islanding operation of AC microgrids," *IEEE Trans. Smart Grid*, vol. 7, no. 1, pp. 200-215, Jan. 2016.

[12] Q. C. Zhong, and T. Hornik, *Control of power inverters in renewable energy and smart grid integration*, John Wiley & Sons, vol. 97, 2012.

[13] Y. W. Li and C. N. Kao, "An accurate power control strategy for power-electronics-interfaced distributed generation units operating in a low-voltage multi-bus microgrid," *IEEE Trans. Power Electron.*, vol. 24, no. 12, pp. 2977-2988, Aug. 2009.

[14] J. M. Guerrero, L. G. de Vicuna, J. Matas, M. Castilla, and J. Miret, "Output impedance design of parallel-connected UPS inverters with wireless load sharing control," *IEEE Trans. Ind. Electron.*, vol. 52, no. 4, pp. 1126-1135, Aug. 2005.

[15] C.-T. Lee, C.-C. Chu, and P.-T. Cheng, "A new droop control method for the autonomous operation of distributed energy resource interface converters," *IEEE Trans. Power Electron.*, vol. 28, no. 4, pp. 1980-1993, Apr. 2013.

[16] L.-Y. Lu and C.-C. Chu, "Consensus-based droop control of isolated micro-grids by ADMM implementations," *IEEE Trans. Smart Grid*, vol. 9, no. 5, pp. 5101-5112, Sept. 2018.

[17] J. W. Simpson-Porco, Q. Shafiee, F. Dorfler, J. C. Vasquez, J. M. Guerrero, and F. Bullo, "Secondary frequency and voltage control of islanded microgrids via distributed averaging," *IEEE Trans. Ind. Electron.*, vol. 62, no.11, pp. 7025-7038, Nov. 2015.

[18] A. R. Bergen and D. J. Hill, "A structure preserving model for power system stability analysis," *IEEE Trans. Power App. Syst.*, vol. PAS-100, no. 1, pp. 25-35, Jan. 1981.

[19] N. Ainsworth and S. Grijalva, "A structure-preserving model and sufficient condition for frequency synchronization of lossless droop inverter-based AC networks," *IEEE Trans. Power Syst.*, vol. 28, no. 4, pp. 4310-4319, Nov. 2013.

[20] P. Kundur, *Power system stability and control*, New York: McGraw-Hill, 1994.

[21] N. A. Tsolas, A. Arapostathis, and P. P. Varaiya, "A structure preserving energy function for power system transient stability analysis," *IEEE Trans. Circuits Syst.*, vol. 32, no. 10, pp. 1041-1049, Oct. 1985.

[22] Y. Zou, M.-H. Yin, and H.-D. Chiang, "Theoretical foundation of the controlling UEP method for direct transient-stability analysis of network-preserving power system models," *IEEE Trans. Circuits Syst. I: Fundam. Theory Appl.*, vol. 50, no. 10, pp. 1324-1336, Oct. 2003.

[23] M. Ashabani and H. B. Gooi, "Multiobjective automated and autonomous intelligent load control for smart buildings," *IEEE Trans. Power Syst.*, vol. 33, no. 3, pp. 2778-2791, May 2018.

[24] R. Krishnan, *Electric motor drives: Modeling, analysis, and control*, Prentice Hall, 2001.

[25] K. De Brabandere, B. Bolsens, J. Van den Keybus, A. Woyte, J. Driesen, and R. Belmans, "A voltage and frequency droop control method for parallel inverters," *IEEE Trans. Power Electron.*, vol. 22, no. 4, pp. 1107-1115, Jul. 2007.

[26] J. Schiffer and F. Dorfler, "On stability of a distributed averaging pi frequency and active power controlled differential-algebraic power system model," in *Proc. 15th Eur. Control Conf.*, pp. 1487-1492, 2016.

[27] D. J. Hill and I. M. Mareels, "Stability theory for differential/algebraic systems with application to power systems," *IEEE Trans. Circuits Syst.*, vol. 37, no. 11, pp. 1416-1423, 1990.

[28] F. Dorfler, J. W. Simpson-Porco, and F. Bullo, "Breaking the hierarchy: Distributed control and economic optimality in microgrids," *IEEE Trans. Control Netw. Syst.*, vol. 3, no. 3, pp. 241-253, Sept. 2016.
[29] D. P. Bersekas and J. N. Tsitsiklis, *Parallel and distributed computation: Numerical methods*, New York: Athena Scientific, 1997.
[30] T. Erseghe, D. Zennaro, E. Dall Anese, and L. Vangelista, "Fast consensus by the alternating direction multipliers method," *IEEE Trans. Signal Process.*, vol. 59, no. 11, pp. 5523-5537, Nov. 2011.
[31] G. Franca, D. P. Robinson, and R. Vidal, "ADMM and accelerated ADMM as continuous dynamical systems," *International Conference on Machine Learning*, arXiv:1805.06579 [math.OC], Aug. 2018.
[32] Trilliant Inc., The Multi-Tier Smart Grid Architecture. [Online]. Available: http ://www.trilliantinc.com/solutions/multi-tier-architecture/.
[33] The MathWorks, September 2018 (Update January 2019). [Online]. Available: https://mathworks.com

Li Sun received the B. Eng. degree and the M.Eng. degrees from Huazhong University of Science and Technology (HUST), Wuhan, China, in 2013, and 2016 respectively, and the Ph.D. degree from The University of Hong Kong, Hong Kong, in 2019, both in electrical engineering. Her current research interests focus on the stability control and optimization design for the frequency and power sharing of distributed generation units in microgrids.

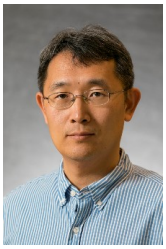

Kai Sun (M06SM13) received the B.S. degree in automation in 1999 and the Ph.D. degree in control science and engineering in 2004 both from Tsinghua University, Beijing, China. He is an associate professor at the Department of EECS, University of Tennessee, Knoxville, USA. He was a project manager in grid operations and planning at the EPRI, Palo Alto, CA from 2007 to 2012. Dr. Sun have served in the editorial boards of IEEE Transactions on Power Systems, IEEE Transactions on Smart Grid, IEEE Access, IEEE Open Access Journal of Power and Energy and IET Generation, Transmission and Distribution.

Yunhe Hou (M'08-SM'15) received the B.E. and Ph.D. degrees in electrical engineering from Huazhong University of Science and Technology, Wuhan, China, in 1999 and 2005, respectively. He was a Post-Doctoral Research Fellow at Tsinghua University, Beijing, China, from 2005 to 2007, and a Post-Doctoral Researcher at Iowa State University, Ames, IA, USA, and the University College Dublin, Dublin, Ireland, from 2008 to 2009. He was also a Visiting Scientist at the Laboratory for Information and Decision Systems, Massachusetts Institute of Technology, Cambridge, MA, USA, in 2010. He has been a Guest Professor with Huazhong University of Science and Technology, China from 2017 and an Adviser of China Electric Power Research Institute from 2019. He joined the faculty of the University of Hong Kong, Hong Kong, in 2009, where he is currently an Associate Professor with the Department of Electrical and Electronic Engineering. Dr. Hou is an Editor of the IEEE Transactions on Smart Grid and an Associate Editor of the Journal of Modern Power Systems and Clean Energy.

Jiabing Hu (S'05M'10SM'12) received the B. Eng. and Ph.D. degrees in College of Electrical Engineering, Zhejiang University, Hangzhou, China, in 2004 and 2009, respectively. From 2007 to 2008, he was funded by Chinese Scholarship Council (CSC) as a visiting scholar with the Department of Electronic and Electrical Engineering, University of Strathclyde, Glasgow, U.K. From April 2010 to August 2011, he was a Post-Doctoral Research Associate with Sheffield Siemens Wind Power (S2WP) research center and the Department of Electronic and Electrical Engineering, University of Sheffield, Sheffield, U.K. Since September 2011, he has been a professor with State Key Laboratory of Advanced Electromagnetic Engineering and Technology, and School of Electrical and Electronic Engineering, Huazhong University of Science and Technology, Wuhan, China. His current research interests include grid-integration of large-scale renewables, and modeling, analysis and control of power electronized power systems. Dr. Hu serves as an Editor of IEEE Transactions on Energy Conversion, an Associate Editor of IET Renewable Power Generation, and a member of Editorial Board for Automation of Electric Power Systems. He is the co-convenor of IEC SC8A JWG5 and an active expert of IEC SC8A WG1/AHG3. He was nominated in 2016, 2017 and 2018 by Elsevier to be between the 40 Most Cited Chinese Researchers in electrical and electronic engineering. He is the Fellow of Institute of Engineering and Technology (IET).